Thermal Radiation Effects on the Mixed Convection Stagnation-Point Flow in a Jeffery Fluid

Tasawar Hayat[a,b], Sabir Ali Shehzad[a], Muhammad Qasim[a], and Saleem Obaidat[b]

[a] Department of Mathematics, Quaid-I-Azam University 45320, Islamabad 44000, Pakistan
[b] Department of Mathematics, College of Sciences, King Saud University, P.O. Box 2455, Riyadh 11451, Saudi Arabia

Reprint requests to M. Q.; Tel: +92 51 90642172; E-mail: mq_qau@yahoo.com

Z. Naturforsch. **66a,** 606 – 614 (2011) / DOI: 10.5560/ZNA.2011-0024
Received September 27, 2010 / revised June 7, 2011

This study describes the mixed convection stagnation point flow and heat transfer of a Jeffery fluid towards a stretching surface. Mathematical formulation is given in the presence of thermal radiation. The Rosseland approximation is used to describe the radiative heat flux. Similarity transformations are employed to reduce the partial differential equations into the ordinary differential equations which are then solved by a homotopy analysis method (HAM). A comparative study is made with the known numerical solutions in a limiting sense and an excellent agreement is noted. The characteristics of involved parameters on the dimensionless velocity and temperature are also examined. It is noticed that the velocity increases with an increase in Deborah number. Further, the temperature is a decreasing function of mixed convection parameter. We further found that for fixed values of other parameters, the local Nusselt number increases by increasing suction parameter and Deborah number.

Key words: Mixed Convection; Stagnation-Point Flow; Thermal Radiation; Jeffery Fluid; Series Solutions.

1. Introduction

Considerable attention has been directed in the past to the boundary layer flows of non-Newtonian fluids. Such fluids are quite common in process of manufacturing coated sheets, foods, optical fibers, drilling muds, plastic polymers etc. The relationships between the shear stress and flow field in these fluids are very tedious and thus offer interesting challenges to the researchers. Inspite of all these challenges, the researchers in the field are even making valuable contributions in the investigations of non-Newtonian fluids [1 – 15].

The flow and heat transfer over a stretching surface is important in the process of extrusion, paper production, insulating materials, glass drawing, continuous casting, fine-fiber matts etc. Several attempts regarding the stretching and stagnation-point flows have been made under various aspects. Convective heat transfer further plays a vital role in nuclear power plants, gas turbines, and various propulsion devices for aircraft, missiles, satellites, and space vehicles and in several engineering applications. Thermal radiation on heat transfer processes are useful in the design of many advanced energy conservation systems operating at high temperature. Chiam [16] studied the two-dimensional stagnation-point flow of a viscous fluid towards a linear stretching surface. Mahapatra and Gupta [17] discussed the heat transfer in the stagnation point flow towards a stretching surface. The steady stagnation point flow of an incompressible micropolar fluid bounded by a stretching surface is presented by Nazar et al. [10]. Xu et al. [18] performed computation for an unsteady flow of hydrodynamic power law fluid near a stagnation point flow. Sadeghy et al. [19] numerically studied the stagnation point flow of an upper convected Maxwell fluid. Hayat et al. [20] investigated the magnetohydrodynamic (MHD) flow of a microploar fluid near the stagnation point flow of a micropolar fluid near a stagnation point. Ishak et al. [21, 22] investigated the mixed convection stagnation point flow of an incompressible viscous fluid towards a vertical permeable stretching sheet. The effect of thermal radiation on mixed convection boundary layer magnetohydrodynamic stagnation point flow in a porous space has been investigated by Hayat et al. [23].

The aim of the current study is two fold. Firstly, to extend the analysis of [21] from viscous to a Jeffrey fluid. Secondly, to provide an analytic solution of the resulting nonlinear system. The series solution of the mathematical problem is derived by the homotopy analysis method (HAM). Previously this method has been successfully applied for other problems [24–32]. The present study is arranged as follows. Section 2 consists of the problem formulation. The series solutions of velocity and temperature are derived in Section 3. Convergence of the obtained series solutions are analyzed in Section 4. Section 5 presents the discussion of plots and tables. Section 6 presents the main conclusions.

2. Problem Formulation

We consider the two-dimensional flow near a stagnation point in the half space $y > 0$. The sheet in the XOZ plane is stretched in the x-direction such that the velocity component in x-direction varies linearly along it. The ambient fluid moves with a velocity ax. The heat transfer effects are taken into account. The velocity $u_\mathrm{w}(x)$ and the concentration $T_\mathrm{w}(x)$ of the stretching sheet is proportional to the distance x from the stagnation-point, where $T_\mathrm{w}(x) > T_\infty$. In the absence of viscous dissipation the equations governing the boundary layer flow can be written as

$$\frac{\partial u}{\partial x}+\frac{\partial v}{\partial y}=0, \tag{1}$$

$$u\frac{\partial u}{\partial x}+v\frac{\partial u}{\partial y}=U_\infty\frac{\partial U_\infty}{\partial x}+\frac{\nu}{1+\lambda_1}\cdot\left[\frac{\partial^2 u}{\partial y^2}+\lambda_2\left(u\frac{\partial^3 u}{\partial x\partial y^2}+v\frac{\partial^3 u}{\partial y^3}-\frac{\partial u}{\partial x}\frac{\partial^2 u}{\partial y^2}+\frac{\partial u}{\partial y}\frac{\partial^2 u}{\partial x\partial y}\right)\right]+g\beta_\mathrm{T}(T-T_\infty), \tag{2}$$

$$u\frac{\partial T}{\partial x}+v\frac{\partial T}{\partial y}=\alpha\frac{\partial^2 T}{\partial y^2}-\frac{\partial q_\mathrm{r}}{\partial y}. \tag{3}$$

In the above equations u, v denote the velocity components along the x- and y-axes, ρ the fluid density, ν the kinematic viscosity, T the temperature, α the thermal diffusivity, c_p the specific heat, k the thermal conductivity of the fluid, g the gravitational acceleration, β_T the thermal expansion coefficient, q_r the radiative heat flux, λ_1 the ratio of relaxation and retardation times and λ_2 is the relaxation time.

Through Rosseland approximation [32], we can write

$$q_\mathrm{r}=-\frac{4\sigma^*}{3k^*}\frac{\partial T^4}{\partial y}, \tag{4}$$

where σ^* is the Stefan–Boltzmann constant, k^* the mean absorption coefficient, and, by Taylor series,

$$T^4 \approx 4T_\infty^3 T-3T_\infty^4. \tag{5}$$

Equations (3)–(5) give

$$\rho c_\mathrm{p}\left[u\frac{\partial T}{\partial x}+v\frac{\partial T}{\partial y}\right]=\frac{\partial}{\partial y}\left[\left(\frac{16\sigma^* T_\infty^3}{3k^*}+\alpha\right)\frac{\partial T}{\partial y}\right]. \tag{6}$$

The appropriate boundary conditions can be expressed as

$$u=u_\mathrm{w}(x)=cx,\ \ v=v_\mathrm{w}(x), \quad T=T_\mathrm{w}(x)=T_\infty+bx \ \text{ at } y=0, \tag{7}$$

$$u=U_\infty(x)=ax,\ T=T_\infty \ \text{ as } y\to\infty, \tag{8}$$

$$v_\mathrm{w}(x)=-\sqrt{c\nu}S \tag{9}$$

with $f(0)=S$ (with $S>0$ for suction and $S<0$ for injection), c is a stretching rate, and the subscripts w and ∞ have been used for the wall and the free stream conditions.

Selecting

$$\eta=\sqrt{\frac{c}{\nu}}y,\ u=cxf'(\eta),\ \ v=-\sqrt{c\nu}f(\eta), \quad \theta=\frac{T-T_\infty}{T_\mathrm{w}-T_\infty}, \tag{10}$$

(1) is satisfied and (2) and (6) reduce to

$$f'''+(1+\lambda_1)(ff''-f'^2)+\beta(f''^2-ff'''')+(1+\lambda_1)\frac{a^2}{c^2}+(1+\lambda_1)\lambda\theta=0, \tag{11}$$

$$\left(1+\frac{4}{3}N_\mathrm{R}\right)\theta''+\mathrm{Pr}(f\theta'-\theta f')=0, \tag{12}$$

$$f=S,\ \ f'=1,\ \ \theta=1 \ \text{ at } \eta=0, \quad f'=\frac{a}{c},\ \ \theta=0 \ \text{ at } \eta\to\infty, \tag{13}$$

where the Deborah number β, the Prandtl number Pr, the radiation parameter N_R, the local Grashof number Gr_x, mixed convection parameter λ, the local Reynold number Re_x, and suction parameter S are

$$\beta=\lambda_2 c,\ \ \mathrm{Pr}=\frac{\mu c_\mathrm{p}}{\alpha},\ \ N_\mathrm{R}=\frac{4\sigma^* T_\infty^3}{k^* k},\lambda=\frac{\mathrm{Gr}_x}{\mathrm{Re}_x^2},$$
$$\mathrm{Gr}_x=\frac{g\beta_\mathrm{T}(T_\mathrm{w}-T_\infty)x^3}{\nu^2},\ \ \mathrm{Re}_x=\frac{u_\mathrm{w}x}{\nu}. \tag{14}$$

The local Nusslet number Nu_x at the wall and q_w are

$$\mathrm{Nu}_x=\frac{xq_\mathrm{w}}{k(T_\mathrm{w}-T_\infty)},\ \ q_\mathrm{w}=-k\left(\frac{\partial T}{\partial y}\right)_{y=0}.$$

The dimensionless variables lead to the expressions given below:

$$\mathrm{Nu}_x/\mathrm{Re}_x^{1/2}=-\theta'(0). \tag{15}$$

3. Series Solutions

In order to proceed for the HAM solutions, we select the base functions

$$\left\{\eta^k\exp(-n\eta),\ \ k\geq 0,\ \ n\geq 0\right\}$$

and write

$$f(\eta)=a_{0,0}^0+\sum_{n=0}^{\infty}\sum_{k=0}^{\infty}a_{m,n}^k\eta^k\exp(-n\eta),$$
$$\theta(\eta)=\sum_{n=0}^{\infty}\sum_{k=0}^{\infty}b_{m,n}^k\eta^k\exp(-n\eta), \tag{16}$$

where $a_{m,n}^k$ and $b_{m,n}^k$ are the coefficients. The initial guesses (f_0 and θ_0) and auxiliary linear operators ($\mathcal{L}_f$, $\mathcal{L}_\theta$) are

$$f_0(\eta)=S+\frac{a}{c}\eta+\left(1-\frac{a}{c}\right)[(1-\exp(-\eta)],$$
$$\theta_0(\eta)=\exp(-\eta), \tag{17}$$

$$\mathcal{L}_f(f)=\frac{\mathrm{d}^3 f}{\mathrm{d}\eta^3}-\frac{\mathrm{d}f}{\mathrm{d}\eta},$$
$$\mathcal{L}_\theta(\theta)=\frac{\mathrm{d}^2\theta}{\mathrm{d}\eta^2}-\theta \tag{18}$$

with

$$\mathcal{L}_f[C_1+C_2\exp(\eta)+C_3\exp(-\eta)]=0,$$
$$\mathcal{L}_\theta[C_4\exp(\eta)+C_5\exp(-\eta)]=0, \tag{19}$$

and C_i $(i=1-5)$ are the arbitrary constants. The embedding parameter is $p\in[0,1]$ and the non-zero auxiliary parameters are h_f and h_θ. The corresponding problems at zeroth order are given by

$$(1-p)\mathcal{L}_f[f(\eta;p)-f_0(\eta)]=$$
$$ph_fN_f[\hat{\theta}(\eta;p),\hat{f}(\eta;p)], \tag{20}$$

$$(1-p)\mathcal{L}_\theta[\theta(\eta;p)-\theta_0(\eta)]=$$
$$ph_\theta N_\theta[\hat{\theta}(\eta;p),\hat{f}(\eta;p)], \tag{21}$$

$$f(\eta;p)|_{\eta=0}=S,\ \ \left.\frac{\partial f(\eta;p)}{\partial\eta}\right|_{\eta=0}=1,$$
$$\left.\frac{\partial f(\eta;p)}{\partial\eta}\right|_{\eta=\infty}=\frac{a}{c}, \tag{22}$$

$$\theta(\eta;p)|_{\eta=0}=1,\ \ \theta(\eta;p)|_{\eta=\infty}=0, \tag{23}$$

$$N_f\left[\hat{\theta}(\eta;p),\hat{f}(\eta;p)\right]=\frac{\partial^3\hat{f}(\eta,p)}{\partial\eta^3}$$
$$+(1+\lambda_1)\left[\hat{f}(\eta,p)\frac{\partial^2\hat{f}(\eta,p)}{\partial\eta^2}-\left(\frac{\partial\hat{f}(\eta,p)}{\partial\eta}\right)^2\right]$$
$$+\beta\left[\left(\frac{\partial^2\hat{f}(\eta,p)}{\partial\eta^2}\right)^2-\hat{f}(\eta,p)\frac{\partial^4\hat{f}(\eta,p)}{\partial\eta^4}\right]$$
$$+(1+\lambda_1)\frac{a^2}{c^2}+(1+\lambda_1)\lambda\hat{\theta}(\eta,p), \tag{24}$$

$$N_\theta[\hat{\theta}(\eta;p),\hat{f}(\eta;p)]=\frac{\partial^2\hat{\theta}(\eta;p)}{\partial\eta^2}$$
$$+\mathrm{Pr}\left[f(\eta;p)\frac{\partial\hat{\theta}(\eta;p)}{\partial\eta}-\hat{\theta}(\eta;p)\frac{\partial f(\eta;p)}{\partial\eta}\right]. \tag{25}$$

The above zeroth-order deformation equations (20) and (21) for $p=0$ and $p=1$ have the following solutions:

$$f(\eta;0)=f_0(\eta),\qquad f(\eta;1)=f(\eta), \tag{26}$$
$$\theta(\eta;0)=\theta_0(\eta),\qquad \theta(\eta;1)=\theta(\eta). \tag{27}$$

We noticed that when p increases from 0 to 1 then $f(\eta,p)$ varies from the initial guess $f_0(\eta)$ to the exact solution $f(\eta)$. Employing Taylor's theorem and (26) and (27), we arrive at

$$f(\eta;p)=f_0(\eta)+\sum_{m=0}^{\infty}f_m(\eta)p^m, \tag{28}$$
$$\theta(\eta;p)=\theta_0(\eta)+\sum_{m=0}^{\infty}\theta_m(\eta)p^m, \tag{29}$$

$$f_m(\eta)=\frac{1}{m!}\left.\frac{\partial^m f(\eta;p)}{\partial\eta^m}\right|_{p=0},$$
$$\theta_m(\eta)=\frac{1}{m!}\left.\frac{\partial^m\theta(\eta;p)}{\partial\eta^m}\right|_{p=0}, \tag{30}$$

where the convergence of the series (28) and (29) depends upon h_f and h_θ. The values of h_f and h_θ are selected such that (28) and (29) are convergent at $p=1$. Hence,

$$f(\eta)=f_0(\eta)+\sum_{m=0}^{\infty} f_m(\eta), \quad (31)$$

$$\theta(\eta)=\theta_0(\eta)+\sum_{m=0}^{\infty} \theta_m(\eta). \quad (32)$$

The deformation problems at the mth order are

$$\mathcal{L}_f[f_m(\eta)-\chi_m f_{m-1}(\eta)]=h_f R_m^f(\eta), \quad (33)$$

$$\mathcal{L}_f[\theta_m(\eta)-\chi_m \theta_{m-1}(\eta)]=h_\theta R_m^\theta(\eta), \quad (34)$$

$$\begin{aligned} &f_m(0)=f'_m(0)=f'_m(\infty)=0,\\ &\theta_m(0)=\theta_m(\infty)=0, \end{aligned} \quad (35)$$

$$\begin{aligned} R_m^f(\eta)&=f'''_{m-1}(\eta)+(1-\chi_m)\left((1+\lambda_1)\frac{a^2}{c^2}\right)\\ &+(1+\lambda_1)\lambda\,\theta_{m-1}(\eta) \quad (36)\\ &+\sum_{k=0}^{m-1}\begin{pmatrix}(1+\lambda_1)\left(f_{m-1-k}\; f''_k-f'_{m-1-k}\; f'_k\right)\\ +\beta\left(f''_{m-1-k}\; f''_k-f_{m-1-k}\; f^{iv}_k\right)\end{pmatrix}, \end{aligned}$$

$$\begin{aligned} R_m^\theta(\eta)&=(1+N_\mathrm{R})\,\theta''_{m-1}(\eta)\\ &+\mathrm{Pr}\sum_{k=0}^{m-1}\left[\theta'_{m-1-k}f_k-\theta_k f'_{m-1-k}\right], \end{aligned} \quad (37)$$

$$\chi_m=\begin{cases}0, & m\le 1,\\ 1, & m>1,\end{cases} \quad (38)$$

and the general solutions are

$$f_m(\eta)=f_m^*(\eta)+C_1+C_2\exp(\eta)+C_3\exp(-\eta), \quad (39)$$
$$\theta_m(\eta)=\theta_m^*(\eta)+C_4\exp(\eta)+C_5\exp(-\eta), \quad (40)$$

with f_m^* and θ_m^* as the particular solutions using (35) one obtains

$$\begin{aligned} &C_2=C_4=0,\;\; C_3=\left.\frac{\partial f_m^*(\eta)}{\partial\eta}\right|_{\eta=0},\\ &C_1=-C_3-f_m^*(0),\;\; C_5=-\theta_m^*(0). \end{aligned} \quad (41)$$

The system of (33)–(35) for $m=1,2,3\ldots$ can be solved by using symbolic software Mathematica.

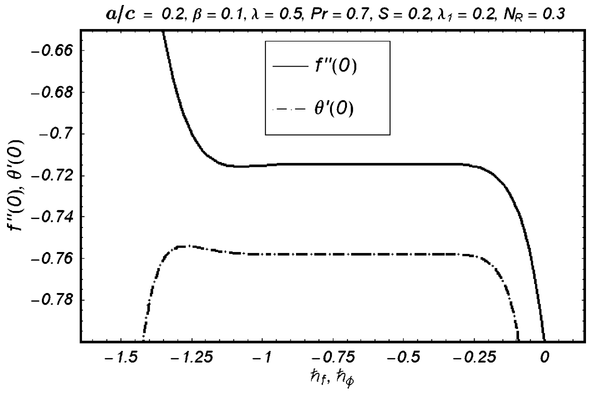

Fig. 1. $\hbar$-curves for 20th order of approximations.

Table 1. Convergence of the series solutions for different order of approximation when $\lambda_1=0.2$, $\beta=0.1$, $a/c=0.2$, $\mathrm{Pr}=0.5=\lambda$.

Order of approximation	$-f''(0)$	$-\theta'(0)$
1	0.78560	0.82850
5	0.75611	0.78263
10	0.75581	0.78319
15	0.75577	0.78315
20	0.75577	0.78315
25	0.75577	0.78315
30	0.75577	0.78315

4. Convergence of Series Solutions

The auxiliary parameters $\hbar_f$ and $\hbar_\theta$ in the series solutions (31) and (32) are very useful in adjusting and controlling the convergence. In order to find the allowed values of $\hbar_f$ and $\hbar_\theta$, the $\hbar_f$, and $\hbar_\theta$-curves are shown for 20th order of approximations. Figure 1 shows that the range for the admissible values of $\hbar_f$ and $\hbar_\theta$ are $-1.0\le\hbar_f\le-0.2$ and $-1.2\le\hbar_\theta\le-0.3$. Further, the series (31) and (32) converge in the whole region of η when $\hbar_f=-0.5$ and $\hbar_\theta=-1$. Table 1 provides the convergence of the homotopy solutions for different order of approximations when $\lambda_1=0.2$, $\beta=0.3$, $a/c=0.1$, $\mathrm{Pr}=0.5$, $\lambda=0.5$.

5. Results and Discussion

This section emphasizes the effects of mixed convection parameter λ, stretching ratio a/c, suction parameter S, Prandtl number Pr, radiation parameter N_R, Deborah number β, and the parameter λ_1 on the velocity and temperature fields. Such effects have been

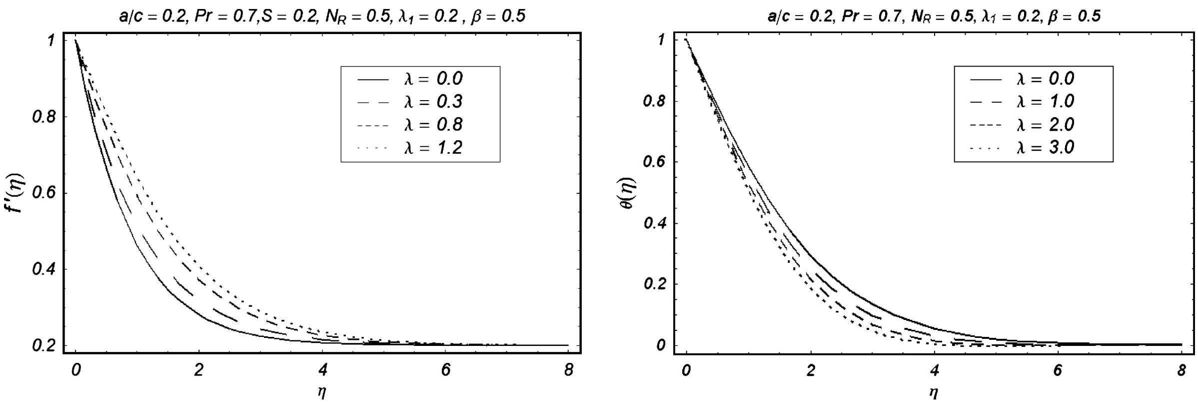

Fig. 2. Influence of λ on f' and θ.

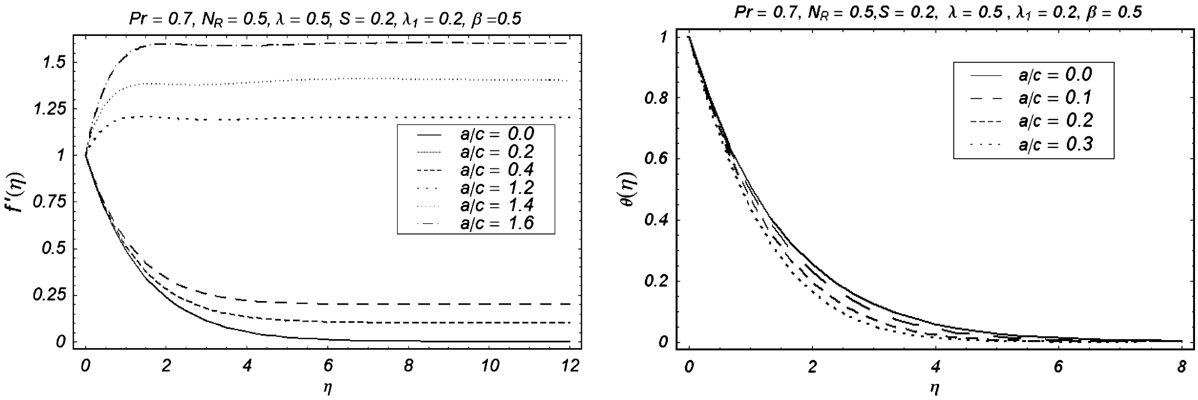

Fig. 3. Influence of a/c on f' and θ.

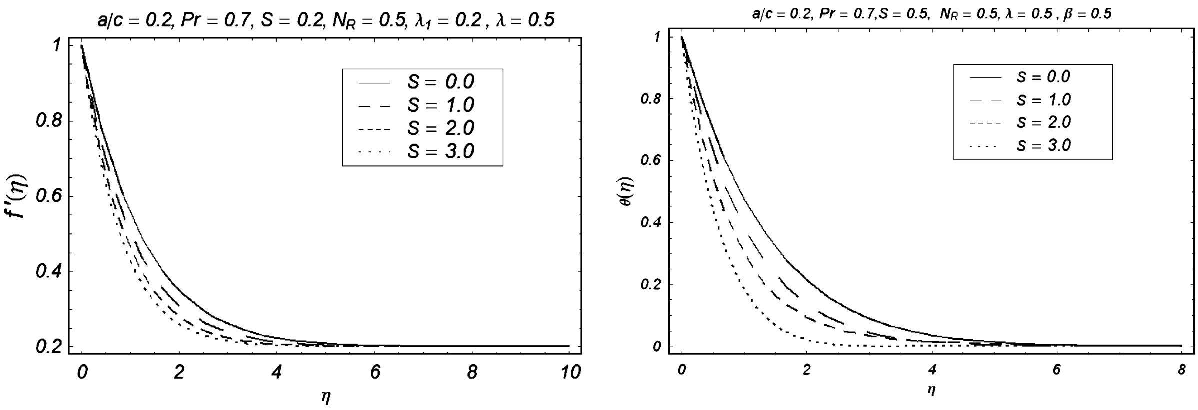

Fig. 4. Influence of S on f' and θ.

displayed in Figures 2 – 8. Figure 2 describes the influence of mixed convection parameter λ on the velocity and temperature profiles, respectively. It is observed that f' is an increasing function of λ. This is due to the fact that increasing values of λ make the buoyancy force stronger and thus increases the velocity. However, an opposite trend is found for the temperature profile θ. The effect of ratio a/c on the ve-

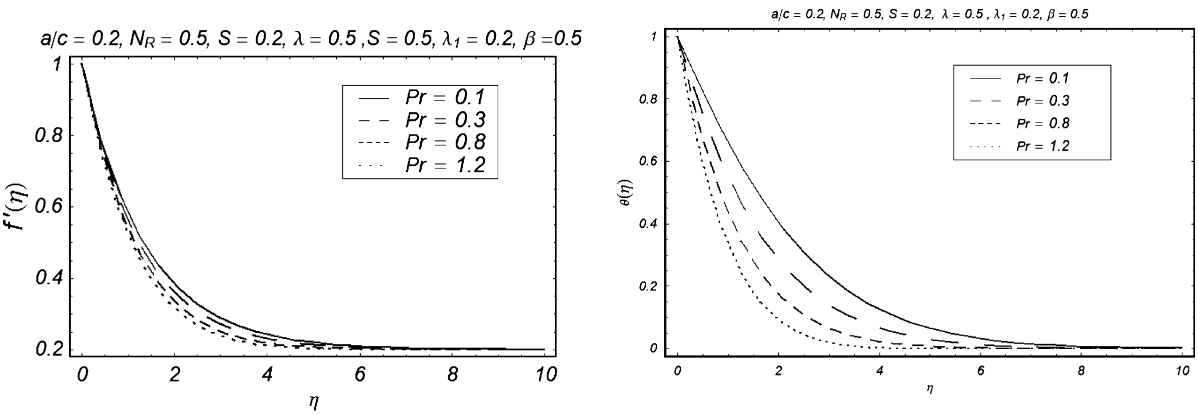

Fig. 5. Influence of Pr on f' and θ.

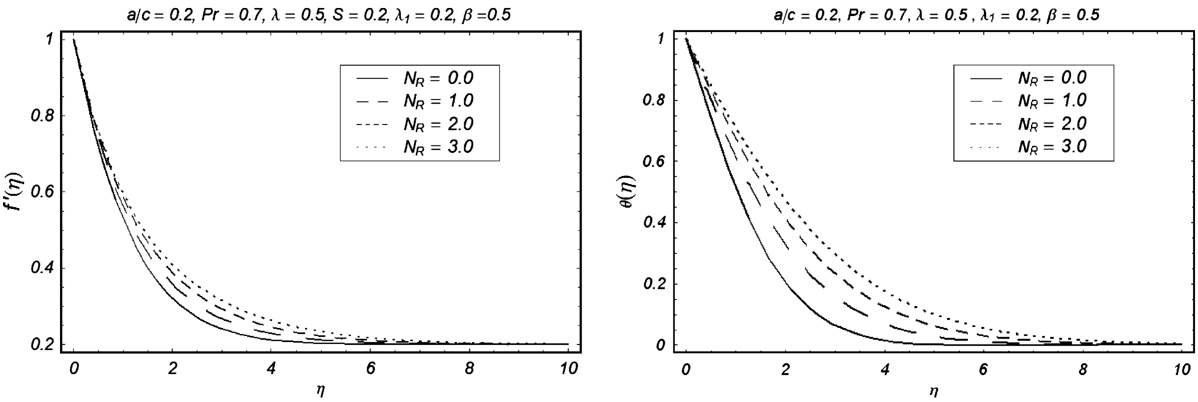

Fig. 6. Influence of N_R on f' and θ.

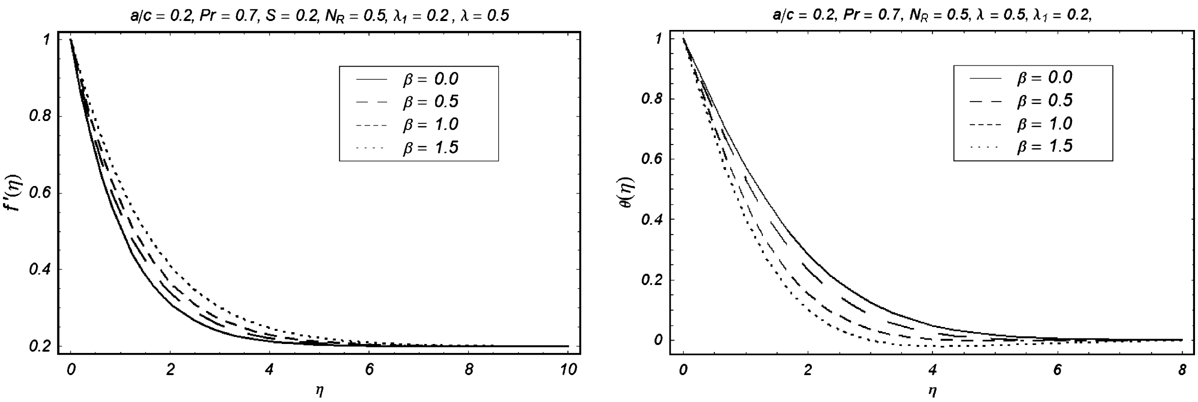

Fig. 7. Influence of β on f' and θ.

locity f' and temperature θ are displayed in Figure 3. The larger values of a/c enhance the free stream velocity. The stronger free stream velocity makes the thermal boundary layer thinner. The influence of suction parameter S is shown in Figure 4. These figures show that velocity and boundary layer thickness are decreasing functions of S. The thermal boundary layer thickness also decreases with S. This is quite in accordance

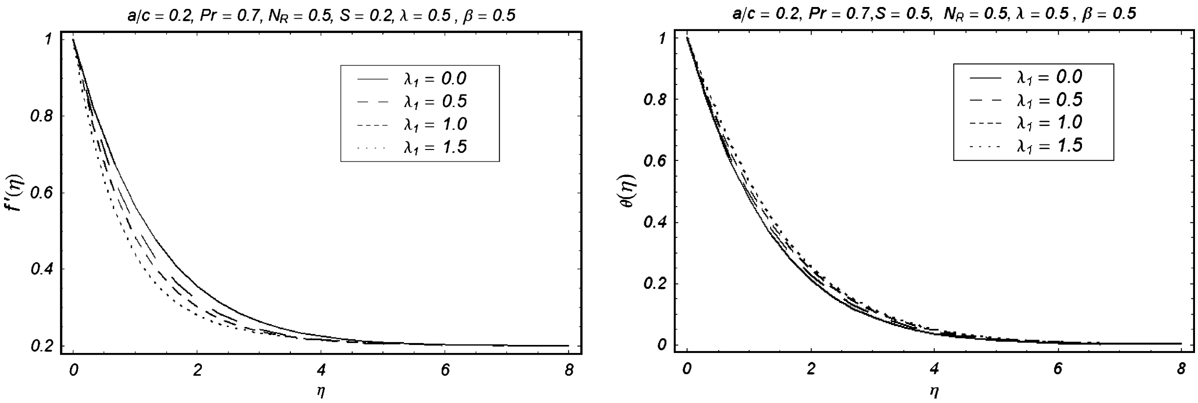

Fig. 8. Influence of λ_1 on f' and θ.

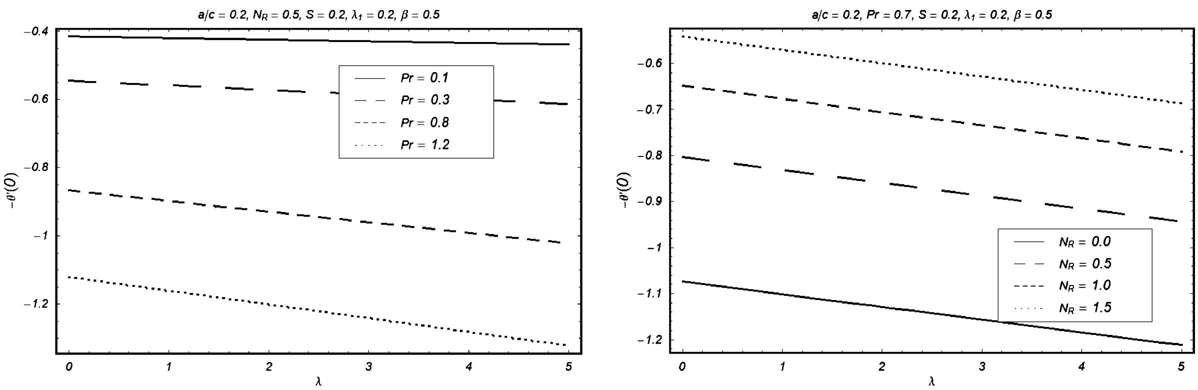

Fig. 9. Variations of the local Nusselt number $-\theta'(0)$ with λ for different values of Pr and N_R.

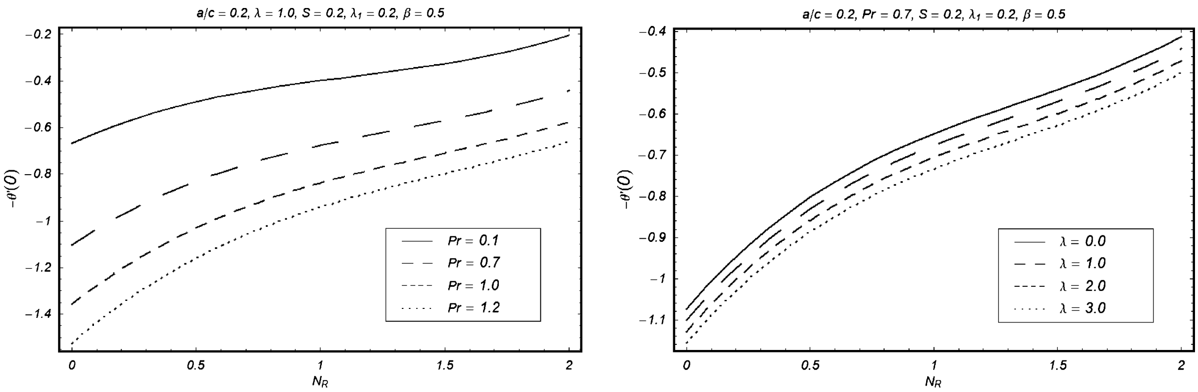

Fig. 10. Variations of the local Nusselt number $-\theta'(0)$ with N_R for different values of Pr and λ.

with the fact that suction causes reduction in the momentum boundary layer thickness. Figure 5 describes the effects of Pr on f' and θ, respectively. Increase in Pr decrease the velocity profile. Infact, an increase in the Prandtl number leads to an increase in fluid viscosity which causes a decrease in the flow velocity. As expected, it is found that θ decreases when Pr increases. A higher Prandtl number fluid has a thinner thermal boundary layer and this increases the gradient of the temperature. Figure 6 clearly indicates that

Table 2. Comparison of values of $f''(0)$ for various values of a/c when Pr = 1, $\lambda = 0$, and $S = 0$.

a/c	[22]	[HAM]
0.01	−0.9980	−0.99823
0.10	−0.9694	−0.96954
0.20	−0.9181	−0.91813
0.50	−0.6673	−0.66735
2.00	2.0175	2.01767
3.00	4.7294	4.72964
10.00	36.2603	36.24021

Table 3. Comparison of values of $-\theta'(0)$ when $a/c = 0$ and $\lambda = 0$.

S	Pr = 0.72		Pr = 1.0		Pr = 10.0	
	[22]	[HAM]	[22]	[HAM]	[22]	[HAM]
−1.0	0.5455	0.54547	0.6181	0.61805	0.9418	0.94167
−0.6	0.6345	0.63462	0.7441	0.74423	1.4709	1.47088
−0.4	0.6866	0.68657	0.8198	0.81944	1.9681	1.96832
−0.2	0.7446	0.74459	0.9050	0.90534	2.7096	2.70945
0.0	0.8088	0.80873	1.0000	1.00000	3.7208	3.72068
0.2	0.8798	0.87975	1.1050	1.10524	4.9765	4.97643
0.4	0.9575	0.95748	1.2198	1.21974	6.4260	6.42598
0.6	1.0420	1.04293	1.3440	1.34434	8.0178	8.01778
1.0	1.2297	1.22965	1.6180	1.61823	11.4762	11.4347

Table 4. Comparison of values of $f''(0)$ for various values of a/c when Pr = 1, $\lambda = 0$, and $S = 0$.

a/c	$\lambda = -0.1$		$\lambda = 1.0$	
	[22]	[HAM]	[22]	[HAM]
0	−1.0513	−1.0513	−0.5608	−0.56076
0.01	−1.0490	−1.0490	−0.5596	−0.55923
0.05	−1.0372	−1.0372	−0.5528	−0.55345
0.10	−1.0176	−1.0176	−0.5398	−0.53982
0.20	−0.9638	−0.9638	−0.5002	−0.50023
0.50	−0.7075	−0.7075	−0.2846	−0.28446
1.0	−0.0343	−0.0343	0.3350	0.33501
2.0	1.9899	1.9899	2.2913	2.29156

Table 5. Comparison of values of $-\theta'(0)$ for various values of a/c when Pr = 1, $\lambda = 0$, and $S = 0$.

a/c	$\lambda = -0.1$		$\lambda = 1.0$	
	[22]	[HAM]	[22]	[HAM]
0	0.9856	0.98545	1.0873	1.08756
0.01	0.9880	0.98834	1.0881	1.08782
0.05	0.9977	0.99725	1.0921	1.09543
0.10	1.0079	1.00737	1.0982	1.09567
0.20	1.0362	1.03623	1.1133	1.15642
0.50	1.1186	1.11898	1.1714	1.17647
1.0	1.2502	1.25127	1.2827	1.28565
2.0	1.4855	1.48523	1.5020	1.51136

Table 6. Values of the surface heat transfer $-\theta'(0)$ when Pr = 0.7 and $N_R = 0.3$.

a/c	β	λ	λ_1	$-\theta'(0)$
0.0	0.1	0.5	0.2	0.74751
0.05				0.76332
0.12				0.78316
0.3				0.80466
0.2	0.0			0.77807
	0.2			0.78767
	0.3			0.79176
	0.4			0.79547
0.2	0.1	0.0		0.73727
		0.3		0.76692
		0.7		0.79745
		1.0		0.81651
0.2	0.1	0.5	0.0	0.79145
			0.1	0.78704
			0.3	0.77956
			0.5	0.77328

an increase in the radiation parameter N_R leads to an increase of the temperature profiles and of boundary layer thickness with N_R. It can be seen from Figure 7 that the velocity field and boundary layer thickness are increasing functions of β. The temperature decreases for larger values of β (Fig. 7). It is observed from Figure 8 that the effect of λ_1 is opposite to the effect of the Deborah number β. The influence of λ_1 is to increase the thermal boundary layer thickness (Fig. 8). Figure 9 shows the variations of the local Nusselt number $-\theta'(0)$ with λ for different values of Pr and N_R, respectively. It is evident from Figure 10 that both the Prandtl number Pr and the mixed convection parameter λ show similar effects on the local Nusselt number, i.e increasing Pr and λ decreases the values of $-\theta'(0)$.

Table 1 is displayed to examine the convergence of series solution which indicates that convergence is achieved at 15th order of approximations. Tables 2–5 show the comparison of the values of HAM solution with the numerical solution in the limiting cases. Table 2 presents the comparison of the values of $f''(0)$ for the various values of a/c. An excellent agreement is noticed between the two solutions in the viscous fluid case. The magnitude of the local Nusselt number increases by increasing suction parameter S (Table 3). The comparison of values of $f''(0)$ for different values of a/c are computed in Table 4. Table 6 shows that the local Nusselt number $-\theta'(0)$ increases by increasing both λ and β.

6. Closing Remarks

Mixed convection stagnation point flow of a Jeffrey fluid towards a stretching sheet is analyzed. Series solution is computed by means of homotopy analysis method. The main observations are listed below.

- The effects of λ and a/c on the velocity profile f' are similar in a qualitative sense.
- The velocity f' increases when β increases.
- The influence of λ is to increase the boundary layer thickness.
- Both f' and θ are decreasing functions of S.
- The temperature θ yields decrease when Pr increases.
- Local Nusselt number is an increasing function of S, λ, a/c, and Pr.

Acknowledgement

Dr. Hayat as a visiting Professor thanks the support of Global Research Network for Computational Mathematics and King Saud University of Saudi Arabia for this work.

[1] C. Fetecau and C. Fetecau, Int. J. Eng. Sci. **44**, 788 (2006).
[2] C. Fetecau, T. Hayat, and C. Fetecau, Int. J. Nonlin. Mech. **41**, 880 (2006).
[3] C. Fetecau, C. Fetecau, M. Kamran, and D. Vieru, J. Non-Newtonian Fluid Mech. **156**, 189 (2009).
[4] W. C. Tan and T. Masuoka, Int. J. Nonlin. Mech. **40**, 512 (2005).
[5] W. C. Tan and M. Y. Xu, Mech. Res. Commun. **29**, 3 (2002).
[6] P. D. Ariel, Int. J. Numer. Meth. Fluid **14**, 757 (1992).
[7] B. Sahoo, Commun. Nonlin. Sci. Numer. Simul. **15**, 602 (2010).
[8] T. Hayat and M. Qasim, Int. J. Numer. Meth. Fluids **66**, 820 (2011).
[9] S. J. Liao, Fluid. Mech. **488**, 189 (2003).
[10] R. Nazar, N. Amin, D. Filip, and I. Pop, Int. J. Nonlin. Mech. **39**, 1227 (2004).
[11] T. Hayat and M. Qasim, Int. J. Heat Mass Transfer **53**, 4780 (2010).
[12] M. Yurusoy and M. Pakdemirli, Mech. Research Commun. **26**, 171 (1999).
[13] R. Cortell, Chem. Eng. Proc. **46**, 721 (2007).
[14] T. Hayat, M. Awais, M. Qasim, and A. A. Hendi, Int. J. Heat Mass Transfer **54**, 3777 (2011).
[15] T. Hayat, M. Qasim, and Z. Abbas, Int. J. Numer. Math. Fluids **66**, 194 (2011).
[16] T. C. Chiam, J. Phys. Soc. Jpn. **63**, 2443 (1994).
[17] T. R. Mahapatra and A. S. Gupta, Heat Mass Transfer, **38**, 517 (2002).
[18] H. Xu, S. J. Liao, and I. Pop, J. Non-Newtonian Fluid Mech. **139**, 31 (2006).
[19] K. Sadeghy, H. Hajibeygi, and S. M. Taghavi, Int. J. Nonlin. Mech. **41**, 1242 (2006).
[20] T. Hayat, T. Javed, and Z. Abbas, Nonlin. Analysis: Real World Appl. **10**, 1514 (2009).
[21] A. Ishak, R. Nazar, and N. M. Arifin, Malaysian. J. Math. Sci. **2**, 217 (2007).
[22] A. Ishak, R. Nazar, N. Bachok, and I. Pop, Phys. A **389**, 40 (2010).
[23] T. Hayat, Z. Abbas, I. Pop, and S. Asghar, Int. J. Heat Mass Transfer **53**, 466 (2010).
[24] S. J. Liao, Beyond Perturbation: Introduction to Homotopy Analysis Method, Chapman and Hall, CRC Press, Boca Reton 2003.
[25] S. J. Liao, Commun. Nonlin. Sci. Numer. Simul. **14**, 2144 (2009).
[26] T. Hayat, M. Qasim, and Z. Abbas, Commun. Nonlin. Sci. Numer. Simul. **15**, 2375 (2010).
[27] T. Hayat, M. Qasim, and Z. Abbas, Z. Naturforsch. **65a**, 231 (2010).
[28] T. Hayat, M. Qasim, Z. Abbas, and A. A. Hendi, Z. Naturforsch. **64a**, 1111 (2010).
[29] T. Hayat and M. Qasim, Z. Naturforsch. **64a**, 950 (2010).
[30] M. Dehghan and R. Salehi, Z. Naturforsch. **66a**, 259 (2011).
[31] T. Hayat, S. A. Shehzad, M. Qasim, and S. Obaidat, Z. Naturforsch. **66a**, 417 (2011).
[32] A. Ishak, Chin. Phys. Lett. **26**, 034701 (2009).